Physics of the Solid State, 2025, Vol. 67, No. 5

01,13

Volume-temperature dependence of electrical resistivity and thermal conductivity of vanadium at high pressures

© A.M. Molodets, A.A. Golyshev, V.V. Kim

Federal Research Center of Problems of Chemical Physics and Medicinal Chemistry RAS,
Chernogolovka, Russia

E-mail: molodets@icp.ac.ru

Received April 10, 2025
Revised May 7, 2025
Accepted May 7, 2025

Experimental and computational results of a study of the volume-temperature dependence of the electrical resistivity of vanadium at high pressures and elevated temperatures are presented. The experimental part of the work contains measurements of the electrical resistance of shock-compressed vanadium samples under stepwise cyclic shock compression in the pressure range up to 70 GPa and temperatures up to 750 K. Calculations of the history of the thermodynamic state of shock-compressible vanadium have been carried out. It is shown that the saturation effect of the electrical resistivity of vanadium, which occurs at atmospheric pressure, persists at gigapascal pressures. A semi-empirical interpretation of the regularities of the volume-temperature dependence of the electrical resistivity and thermal conductivity of vanadium is formulated, which makes it possible to predict these properties up to pressures in the gigapascal range.

Keywords: saturation of electrical resistivity, high pressures, shock compression, thermal conductivity.

DOI: 10.61011/PSS.2025.05.61481.75-25

1. Introduction

It is well known (see [1,2]) that the growth of electrical resistivity of many metals and alloys slows down as the temperature increases. This effect is visualized in the form of an s-shaped curve of temperature vs. electrical resistivity with saturation at high temperatures. Saturation of the resistivity-temperature dependence of metallic materials is justified theoretically by the Ioffe–Regel criterion, where the maximum electrical resistivity of a metal is achieved as the conductivity electron free path approaches the interatomic spacing in this metal.

Besides the apparent theoretical interest, electrical resistivity saturation of particular metals plays an important role, for example, in geophysical applications, when attempts are made to estimate the electronic component of thermal conductivity of planetary interiors at high pressures on the basis of the Wiedemann–Franz law (see [3] and references therein).

For vanadium having the electrical resistivity-temperature dependence effect, there is a vast avalanche of appropriate experimental data (see [4] and reference therein). However note that the high-temperature data regarding the vanadium resistivity as shown in [4] was acquired only at atmospheric pressure, while there is no information in the available literature concerning the electrical resistivity saturation in this metal at high pressures.

According to this make introduction, the objective of our work was to perform an experiment-calculation study of electrical resistivity saturation effect in vanadium at high pressures followed by the reconstruction of volume-temperature dependence of electrical resistivity and thermal conductivity vanadium in pressures ranging within 20–60 GPa.

2. Measurement of electrical resistance of shock-compressed vanadium samples

2.1. Samples and measuring cell

The test samples were made of the VnPl-2 vanadium foil. According to the specification (TU 48-4-373-76), the VnPl-2 vanadium foil contains maximum amounts of the following controlled impurities 0.25 % Fe, 0.3 % Al, 0.3 % Si, 0.02 % N, 0.001 H, 0.05 % O, 0.04 % C. A piece of vanadium foil was used to form a zigzag-shaped tape sample. Width a_0 and thickness h_0 of vanadium samples a_0 were $a_0 = 1.2-1.5$ mm and $h_0 = 0.06-0.08$ mm. Material of the samples in the initial state was in the form of polycrystalline vanadium with body-centered cubic (BCC) lattice.

Measuring cell components of the sample are indicated by numbers *1–3* in Figure 1. Here, current conductors *2* in the form of copper foil 0.015 mm in thickness and 3 mm in width were spot welded to the tape sample ends *1*. Tape sample plane was parallel to the shock wave front plane. A measuring cell of a manganin sensor was placed in the same plane *4, 5*. It means that the manganin sensor cell served as an equivalent of the samples measuring cell, in which the vanadium sample is replaced with a manganin tape sample.

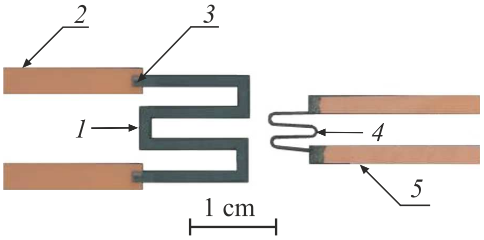

Figure 1. Measuring cell: *1* — vanadium sample, *2* — copper conductors, *3* — copper-vanadium contacts, *4* — sensing element of the manganin pressure sensor, *5* — copper current conductors.

Initial resistances R_0 of vanadium and manganin tape samples were preliminary measured for each experiment and were equal to $\approx 0.5\,\Omega$ for vanadium and to $\approx 1.5\,\Omega$ for manganin.

2.2. Stage-cyclic shock-wave loading generator

A series of shock-wave experiments was conducted for *in situ* resistance measurement of shock-compressed vanadium samples using a stage-cyclic shock-wave loading generator shown in Figure 2. Here, steel impactor *1* is accelerated by explosion products to the velocity W_0. The target is composed of shock anvils consisting of two „hard" steel plates *2* and *4*, and a „soft" insulator layer *3* between them. Insulator *3* consists of a set of PTFE films bonded together with vacuum grease. PTFE film is a 0.1–0.5 mm non-oriented PTFE tape. A thin (compared with the insulator thickness) tape test sample *5* was positioned in the insulator in such a way that its center is placed at the distance H_s from the plate surface *4*. Tape manganin pressure sensor *6* is in the same plane. H_s was varied using a required set of polytetrafluoroethylene films bonded together by micron-thick vacuum grease layers. The caption to Figure 2 shows the specifications of the plates for the optimum experiment series discussed below.

Operation of the shock-wave loading generator is explained in Figure 3. Preliminary, mention should be made of a well-known stage shock-wave compression scheme, considering the disturbance paths in the distance–time coordinates (see Figure 3, *a*) in conjunction with the pressure profile *1* (see Figure 3, *b*) in a Lagrangian particle H_s of a sample made of PTFE, rather than of „hard" metal.

In Figure 3, *a*, a single shock wave path formed after the contact between the impactor and plate *2* is indicated by an arrow with symbol D. At time t_0, a gap at the metal *2*–PTFE *3* interface is disintegrated, then the primary shock wave propagates in insulator *3* at the velocity D_1 and pressure P_1 downstream of the wave front. At time t_r, two shock waves D_2 and D_r with amplitudes P_2 are formed at the PTFE *3*–metal *4* interface. Shock wave D_2 is reflected from plate *2* by shock wave D_3 with pressure P_3 downstream of the wave front.

Further, the cycle of stages P_1–P_3 with the amplitudes of the 4th and following stages P_{3+i} is repeated. With time approaching some point $t_{\max}$, amplitudes P_{3+i} tend to $P_{\max}$

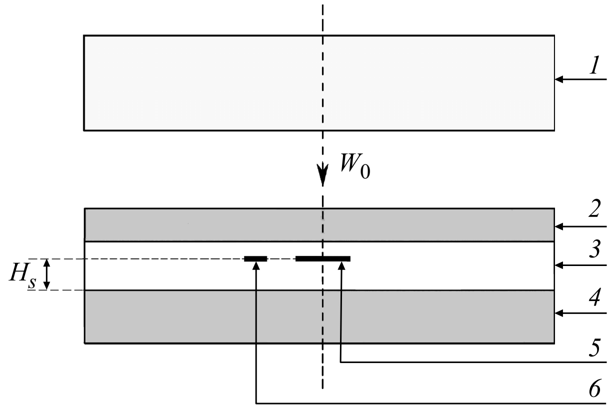

Figure 2. Stage-cyclic shock-wave loading generator: *1* — 3.5 mm steel (stainless steel 18-8) plate impactor with $W_0 = 2.63$ km/s; *2* — 1.85 mm steel (steel 18-8) plate; *3* — a set of PTFE films with a total thickness of 2.34 mm; *4* — 4.08 mm steel (steel 18-8) plate; $H_S = 1.12$ mm — location of vanadium sample *5* and of manganin pressure sensor *6*.

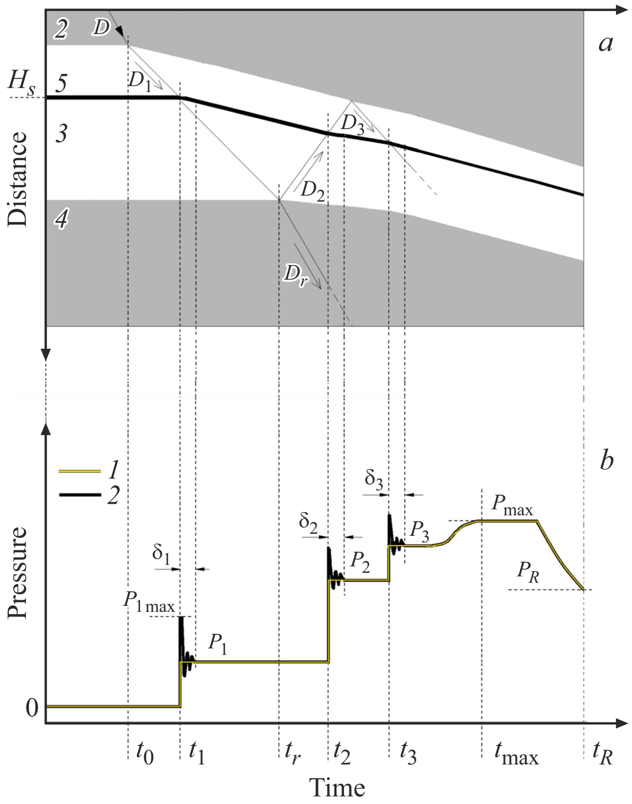

Figure 3. Operation of the stage-cyclic shock loading generator: (*a*) — shock wave kinematics in the distance–time coordinates, meaning of symbols *2, 3, 4, 5*, H_s is the same as in Figure 2; (*b*) — Pressure profile scheme (time dependence) in the plane H_s of the test sample. *1* — simple stage shock compression pressure profile, *2* — stage-cyclic shock compression pressure profile. The rest symbols in Figure 3, *a* and 3, *b* are explained in the text.

that is defined by the impactor velocity and the properties of plates *2, 3, 4*. This stage is shown schematically by a smooth profile section *1* at $P_3 < P < P_{\max}$ in Figure 3, *b*. Ultimately, a pressure profile indicated by*1* in Figure 3, *b* is formed in the sample plane H_s. The shown generator also implies formation of a pressure reduction stage in the sample due to release waves from the rear side of the impactor and free plate surface *4*. This stage occurs at times exceeding $t_{\max}$. This study addresses the shock release only up to t_R and P_R in the shock release wave from the rear side of the striker. Thus, a pressure profile indicated by*1* in Figure 3, *b* is formed in the sample plane H_s.

A stage-cyclic pressure profile (see *2* in Figure 3, *b*) is now discussed for „hard“ metal sample *5*. In this case, when the wave D_1 arrives to the rear side of sample *5* at t_1, a shock wave with $P_{1\,\max}$ starts in the sample. When this wave arrives to the front sample-insulator interface, reverberation of compression and release waves starts in the sample. The reverberation lasts during δ_1 and ends when P_1 is reached in the sample. The same events also take place after t_2 when the wave D_2 arrives to the sample and new wave reverberation starts in the sample. The reverberation lasts during δ_2 and ends when P_2 is reached in the sample. Finally, arrival of the shock wave D_3 stimulates an identical wave reverberation in the sample during δ_3. Reverberation δ_3 ends with formation of the third pressure stage P_3 in the sample and so forth. Reverberations δ_i further occur at the next stage fronts.

Note that the half-period τ_0 of the cyclic component δ is defined as $\tau_0 \sim h_0/C_0$, where h_0 is the sample thickness, C_0 is the speed of sound in the sample material. At $h_0 \sim 0.05\,\mathrm{mm}$ and $C_0 \sim 5\,\mathrm{mm}/\mu$ that are typical for metal samples, τ_0 is equal to $\tau_0 \sim 10\,\mathrm{nc}$. In other words, compression wave reverberations in a thin „hard“ sample surrounded by a „soft“ insulator introduce a submicrosecond cyclic component into each shock compression stage pressure profile. Ultimately, a pressure profile indicated by *2* in Figure 3, *b* is formed in the test sample plane H_s.

Thus, the generator stimulates stage shock-wave loading in the sample that includes a submicrosecond pressure component at each stage front and further smooth pressure reduction.

2.3. Electrical resistance and pressure profiles of shock-compressed vanadium samples

Direct currents $J_0 = 3.0(1)\,\mathrm{A}$ from two independent power supply units were applied along the vanadium and manganin tape samples during shock-wave loading. Electrical resistance variations in the sample and manganin sensor were measured using a two-point scheme with the Wheatstone bridge containing a corresponding measuring cell (see Figure 1) as the resistance to be measured. Measuring cell resistance variation ΔR was treated as the resistance variation sum $\Delta R = \Delta R_1 + \Delta R_2 + \Delta R_3$ of the vanadium sample ΔR_1, copper current conductors ΔR_2 and two copper-sample contact resistances ΔR_3.

The primary experimental information included the profiles (dependences on time t) of bridge unbalance voltage variation $\Delta U = \Delta U(t)$ recorded by the Tektronix DPO4104B high-frequency oscilloscope. Profiles $\Delta U(t)$ were recalculated into the measuring cell resistances using the equation $\Delta R = k\Delta U$, where k is the predetermined calibration coefficient.

As the profile $\Delta R = \Delta R(t)$ contains spurious resistances ΔR_2 and ΔR_3 that are not related to the resistance variation of the test sample, concurrent experiments were conducted to estimate the total resistance variation $\Delta R_2 + \Delta R_3$. For this, profiles $\Delta U = \Delta U(t)$ were measured on a low-resistance measuring cell that consisted of the same components as shown in Figure 1 and differed only in a short length and, consequently, in low resistance of the vanadium sample. Initial resistances of the measuring cell components were: $\approx 0.5\,\Omega$ for the test sample, $\approx 15\,\mathrm{m}\Omega$ for the low-resistance cell sample, $\approx 40\,\mathrm{m}\Omega$ for the copper current conductors, $\approx 1\,\mathrm{m}\Omega$ for each copper-sample contact resistance.

Experiments showed that the total signal profile amplitude ΔR is more than an order of magnitude higher than the resistance variation $\Delta R_2 + \Delta R_3$. On this basis, the spurious contribution of ΔR_2 and ΔR_3 was considered to be insignificant and, thus, the experimental resistance profile of the vanadium sample $R = R(t)$ was calculated as $R = R_0 + \Delta R$, where R_0 is the initial resistance. One of the typical experimental profiles of the series $R = R(t)$ is represented by curve *1* in Figure 4, *a*. The same figure shows signal *2* of the low-resistance cell for comparison. Magnitudes of other complicating effects such as shunting, skin effect, heat exchange between thin metal samples and surrounding insulator are addressed in [5].

Figure 4, *b* shows the pressure profiles in sensitive elements of the measuring cell. Since the manganin sensor has the same thickness and is positioned in the same plane as the sample, its readings vary synchronously with the samples resistance variation. Therefore manganin sensor readings may serve as a time indicator of shock-wave disturbance arrival not only to the manganin sensor, but also to the test sample. In addition, the primary signal of the manganin sensor, being recalculated into the pressure profile (see *1* in Figure 4, *b*), may be used for experimental identification of the stage shock-wave compression profile of the vanadium sample. As for a quantitative pressure profile in the vanadium sample, this profile is calculated according to the procedure described in the next section. The model pressure profile in the vanadium sample for the experiment is shown in Figure 4, *b* as curve *2*.

Further note that model pressure profile *3* in the manganin sample in Figure 4, *b* is similar to model pressure profile *2* in the vanadium sample in that it contains a cyclic component at each stage, while no cyclic component is recorded on experimental profile *1*. This difference of profiles *1* and *3* is caused by a limited frequency response characteristic of the employed resistance measurement technique that is $\approx 100\,\mathrm{MHz}$.

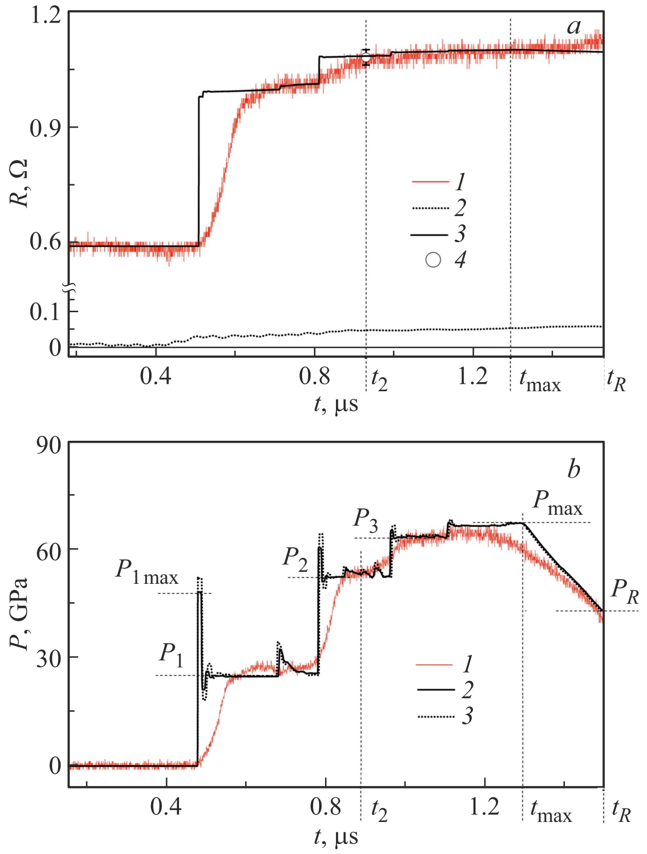

Figure 4. Resistance and pressure in the vanadium sample in stage-cyclic shock compression: (*a*) *1* — experimental resistance profile $R = R(t)$ of the measuring cell, *2* — experimental resistance profile of the low-resistance measuring cell, *3* — model resistance profile $R_{\text{mod}} = R_{\text{mod}}(t)$ of the vanadium sample, *4* — spread in the amplitudes of several experimental profiles $R = R(t)$ at t_2 and P_2, (*b*) *1* — manganin sensor readings in the form of a pressure profile, *2* — model pressure profile $P = P(t)$ in the vanadium sample, symbols P_1, $P_{1\,\text{max}}$, P_2, P_3, P_{max}, P_R, and t_2, t_{max}, t_R have the same meaning as in Figure 3, *b*; *3* — model pressure profile in the manganin sensing element.

3. Reconstruction of the volume-temperature dependence of vanadium resistivity at high pressures and temperatures

Volume-temperature dependences of vanadium resistivity at high pressures and submicrosecond times were reconstructed by concurrent simulation of thermodynamic state history and synchronous resistance variation of the vanadium samples in stage-cyclic shock loading conditions.

3.1. Thermodynamic state simulation of vanadium in stage-cyclic shock-wave loading conditions

Thermodynamic state of vanadium was simulated during the experiments was performed in the hydrocode based on previously developed authors equations of state. For vanadium, the equation of state of the body-centered cubic (BCC) phase o vanadium from [6] were used. For references to works containing the equations of state of the rest materials see [5]. Thermodynamic state simulation of vanadium included elastic-plastic properties in the form of yield strength Y vs. volume $Y = Y(V)$ within the elastoplastic solid body model. As $Y = Y(V)$, data from Table I in [7] were used at constant shear modulus of vanadium $G = 55.2$ GPa.

As the width of the vanadium tape sample a_0 was by an order of magnitude higher than its thickness h_0, then the test sample was simulated in the hydrocode by a plate with the initial thickness h_0. The employed hydrocode allows samples wave interactions and thermodynamic states to be calculated in the form of time dependences (profiles) of pressure $P(t)$, temperature $T(t)$ and specific volume $V(t)$ for any Lagrangian particle of each plate in the multilayer target of the explosion-driven generator in planar one-dimensional shock-wave loading. Thus, calculated profiles $P(t)$, $T(t)$ and $V(t)$ were accepted for the Lagrangian coordinate H_S related to the center of a vanadium plate. As mentioned above, the model pressure profile $P(t)$ for a particular experiment is shown as curve *2* in Figure 4, *b*.

Time exclusion from the calculated profiles $P(t)$ and $T(t)$ provides a phase path in the pressure-temperature coordinates for each experiment. Curve *1* in Figure 5 shows the phase path (thermodynamic history) of stage-cyclic compression in the experiment with $W_0 = 2.63$ km/s. Comments are provided here regarding the position of calculated path *1* in contrast to the previous vanadium shock compression data from [6–8]. As shown, the first stage-cyclic loading shock wave $P_{1\,\text{max}} = 49$ GPa brings vanadium

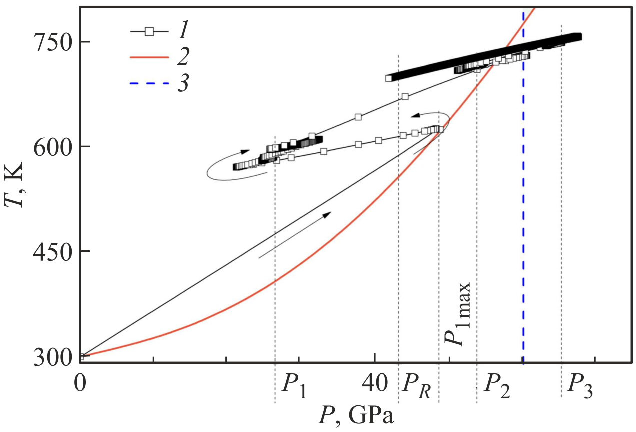

Figure 5. Experimentally studied region of the phase diagram of vanadium in the temperature T — pressure P coordinates: *1* — vanadium phase path in stage-cyclic shock loading, arrows indicate vanadium state sequences TP during the stage-cyclic shock loading process; *2* — design shock adiabat of single-stage shock compression of vanadium from [6]; *3* — equilibrium line between BCC and rhombohedral phases of vanadium from [8]; $P_{1\,\text{max}}$, P_1, P_2, P_3, P_R, the same as in Figure 4, *b*.

to a state in which the yield strength of vanadium is close to zero as specified in [7]. Consequently, $P_{1\,\max}$ lies almost single-stage shock compression adiabat *2* of vanadium from [6]. It can be also seen that a long section of model path *1* is in the vanadium BCC phase region, i. e. to the left of the equilibrium line *3* [8].

Thus, the thermodynamic state simulation data for shock-compressed vanadium makes it possible to indicate the experimentally studied region of the vanadium BCC phase diagram in the temperature range of 580–730 K and pressure range of 20–60 GPa.

3.2. Simulation of volume-temperature dependence of vanadium resistivity

The simulated volume (V) — temperature (T) dependence of resistivity $\rho = \rho(V, T) \propto \rho_0 \varphi \varepsilon$ used a relation in the form of product of the initial resistivity $\rho_0 = \rho(V_0, T_0)$ and two functions: volume component $\varphi = \varphi(V)$ and temperature component $\varepsilon = \varepsilon(T)$.

A power function from [9] characterized by the magnitude of n was used as the volume component prototype $\varphi = \varphi(V)$. Functional view $\varphi = \varphi(V)$ from [9] was modified according to the data from [10] and further used in [11] and in this work as

$$\varphi = \left(\frac{V}{V_0}\right)^{n/3} \left(\frac{\nu_0 - V}{\nu_0 - V_0}\right)^{-2n}, \tag{1}$$

where ν_0 is the individual parameter of the metal, V_0 is the metal specific volume at room temperature T_0 and atmospheric pressure P_0, ν_0 and V_0 are the known parameters from the equations of state. For vanadium, they were taken from [6] and are shown in the table. n has the same meaning as in the prototype [9]. Magnitude of n is determined as specified in [9] through the conductivity electron scattering mechanism in metals and, for example, $n = 2$ is typical of the free electron model in an ideal metal.

Previously, work [11] used the empirical function $\varepsilon = x/\big(\exp(x) - 1\big)$ for the temperature component of metal resistance with saturation, where $x = \theta_\varepsilon / T$, θ_ε is the adjustable coefficient. However, the second adjustable parameter was needed for vanadium. Consequently, for vanadium, expression $\varepsilon = \varepsilon(T)$ was accepted with two adjustable parameters α and θ_ε written as

$$\varepsilon = T^{\alpha} / \exp\left(\frac{\theta_\varepsilon}{T}\right). \tag{2}$$

Taking into account (1) and (2), the model relation for the volume-temperature dependence of the resistivity $\rho = \rho(V, T)$ of metal with resistance saturation is written as

$$\rho = \rho_0 \varphi \varepsilon / \varepsilon_0, \tag{3}$$

where $\rho_0 = \rho(V_0, T_0)$ is the electrical resistivity of the material at atmospheric pressure, volume V_0 and temperature T_0.

$$\varepsilon_0 = T_0^{\alpha} / \exp\left(\frac{\theta_\varepsilon}{T_0}\right).$$

Thus, in terms of model (3), the volume-temperature dependence of resistance with saturation is characterized by a constant initial resistivity of metal ρ_0 and three adjustable parameters: α, θ_ε and n.

3.3. Determining the vanadium resistivity saturation model parameters at high pressures and temperatures

Note that vanadium volume variation is low at atmospheric pressure, and therefore the temperature component parameters α and θ_ε may be determined on the basis of experimental temperature dependence of vanadium resistance. Thus, for example, approximation of the experimental atmospheric isobar of vanadium resistivity [4] using (3) at $V = \text{const} = V_0$, $\rho_0 = 20.21\,\mu\Omega \cdot \text{cm}$, $T_0 = 300\,\text{K}$ gives $\alpha = 0.680(3)$ and $\theta_\varepsilon = 145(2)\,\text{K}$. These values together with the coefficient of determination $R^2 = 0.99997$ were found by the least-square method. Corresponding model curve (3) is indicated by *1* in Figure 6, *a*. It can be seen that curve *1* agrees to a high degree of accuracy with experiment [4] in a broad temperature range.

To determine n, reference data is required not only at great temperature variation, but also at significant vanadium volume variation. The mentioned above resistivity profiles $R = R(t)$ of the shock-compressed vanadium samples may serve as such data. In this case, the desired value fitting algorithm for adjustable parameters involves the following. First, (3) is used to formulate an expression for the model resistance profile of the shock-compressed sample $R_{\text{mod}} = R_{\text{mod}}(t)$ in the planar one-dimensional compression conditions as follows

$$R_{\text{mod}} = \left(\frac{R_0}{\varepsilon_0}\right) \left(\frac{V_0}{V}\right) \varphi \varepsilon, \tag{4}$$

where R_0 is the initial resistance of the sample at room temperature $T_0 = 300\,\text{K}$ and atmospheric pressure P_0, (V_0/V) accounts for the flat sample thickness variation in planar one-dimensional deformation. The rest terms in (4) are the same as in (3). Substitution of the above model profiles of $T = T(t)$ and $V = V(t)$ into (4) provides the model profile $R_{\text{mod}} = R_{\text{mod}}(t)$ that depends on α, θ_ε, n contained in (3). Then „manual“ fitting is used to find such values of free parameters, at which the model resistance profile of the shock-compressed vanadium sample $R_{\text{mod}} = R_{\text{mod}}(t)$ appears to be as near as possible to the experimental one $R = R(t)$.

This algorithm is implemented as shown in curve *3* in Figure 4, *a*. Agreement between the model and experimental profiles was achieved by means of α and n variation with constant $\theta_\varepsilon = 145\,\text{K}$. Optimum values of the desired parameters appeared to be as follows $\alpha = 0.63$ and $n = 2.0$. As shown in Figure 4, *a*, deviation of model profile *3* from experimental profile *1* is maximum 2 %.

To be clear, high submicron peaks could have been expected here at the model stage resistance profile fronts *3* in Figure 4, *a* similar to model pressure profiles in Figure 4, *b*.

Model function coefficients for resistance and heat conductivity of BCC−vanadium

Vanadium	ρ_0, $\mu\Omega \cdot$ cm	T_0, K	V_0, cm^3/mol	v_0, cm^3/mol	n	α	θ_ε, K	ε_0	k_{0l}, W/mK
bcc-V	20.21	300.0	8.35	29.507	2.0	0.63	145(2)	22.42	3.7

However, model profile stage fronts *3* dont contain this feature. The absence of cyclic component at the profile stage fronts *3* results from the compensation of competing contributions of the volume component $\varphi = \varphi(V)$ and temperature component $\varepsilon = \varepsilon(T)$ of the resistance in (4).

Turning back to determining the adjustable parameters, note that the magnitude of α and n was determined by fitting the model profile $R_{\text{mod}} = R_{\text{mod}}(t)$ to the single experimental profile. Therefore the spread of α and n resulting from the spread of $R = R(t)$ will be estimated. The degree of this effect will be estimated on the basis of the spread of amplitudes of several profiles $R = R(t)$ of the identical experiments at t_2 and P_2 indicated by dot *4* in Figure 4, *a*. For this, a number of profiles $R_{\text{mod}} = R_{\text{mod}}(t)$ will be calculated with various values of α and constant $n = 2.0$. It turns out that with variation of α within$\alpha = 0.62-0.64$ the model profiles, while maintaining their shape, dont go beyond the boundaries indicated by dot *4* in terms of amplitude. The same practice was used to estimate the spread of n within $n = 1.9-2.1$ at constant $\alpha = 0.63$. As this parameter varied, variations of $R_{\text{mod}} = R_{\text{mod}}(t)$ were 1 % maximum.

The full set of parameters for the model with saturation of the volume-temperature dependence of vanadium resistance at high pressures and temperatures in the form of (3) is shown in the table.

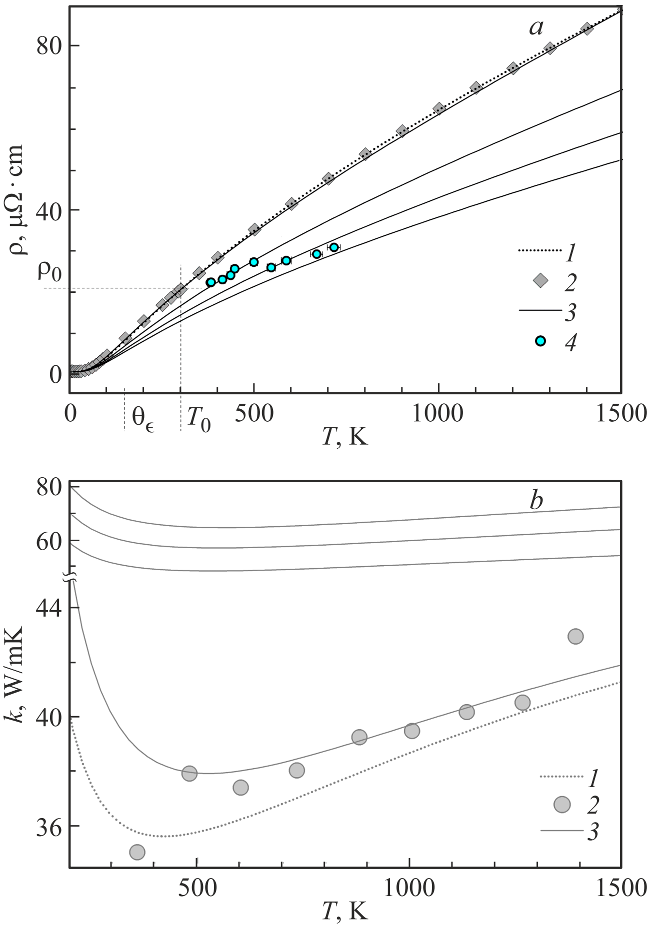

Figure 6. High-temperature isobars of vanadium resistivity and thermal conductivity: (*a*) *1* — approximation of the atmospheric isobar $\rho = \rho(V_0, T)$, *2* — recommended experimental values for the atmospheric isobar from [4], *3* — model resistivity isobars (3) of vanadium $\rho = \rho(V, T)$ at various pressures (from top to bottom) 0.0, 20.0, 40 and 60.0 GPa, *4* — experiment [12]; (*b*) *1* — model isobar of electronic component of thermal conductivity k_e, *2* — experimental data [13], *3* — model isobars of thermal conductivity coefficient (5) at various pressures (from bottom to top) 0.0, 20.0, 40 and 60.0 GPa.

4. Results and discussion

As mentioned above, according to the data in [7], vanadium shows elastoplastic behavior in shock-wave loading. Therefore, taking into account a well known fact of irreversible variation of metal resistance due to formation of defects in plastic deformation, validity of model (3) shall be discussed with respect to vanadium in the completed experiment conditions. Actually, relations (1)−(3) imply that variation of metal resistivity only depends on volume and temperature. Thus, it is assumed, first, that the volume-temperature variation of metal resistivity is reversible and, second, the reversible resistance variation prevails over the irreversible resistance component caused by plastic deformation. Lets consider the arguments in favor of validity of this approximation.

Figure 6, *a* shows the model atmospheric isobar of resistivity $\rho = \rho\big(V(T, P_0), T\big)$ calculated using the tabular parameters and taking into account the variations of vanadium volume during heating. It is shown that the model atmospheric isobar is virtually identical to approximation *1* of static experimental data *2* obtained without plastic deformation of the samples. Thus, the found n and θ_ε turn out to be applicable not only to plastically deformed vanadium along its shock loading phase paths, but also along the high-temperature atmospheric isobar of vanadium in static conditions without plastic deformation. This fact justifies neglecting of vanadium resistance variation due to plastic deformation in planar one-dimensional shock compression.

Soundness of the assumption that the volume-temperature variation of shock-compressed vanadium resistivity is reversible is supported by the explanation of the difference in vanadium sample resistance in Figure 4, *a* in compression and release. Actually, it is shown that coinciding amplitudes of experimental *1* and model *3* resistance profiles increase as the pressure increases to $P_{\max}$, but vary very little at $t_{\max} < t < t_R$, when the pressure decreases significantly in the release wave from $P_{\max}$ to P_R. In terms of model (3), this difference is explained by the above-mentioned consideration of the competing contributions of volume component (1) and component (2) with temperature saturation that use a single set of model parameters θ_ε, α and n. Thus, the fact that the model and experimental resistance profiles coincide in Figure 4, *a* supports that the shock-compressed vanadium resistance is reversible with respect to the volume and temperature variations that occur both in compression and release.

The proposed model description of the volume-temperature dependence of the vanadium resistance in conjunction with the equation of state allows the vanadium resistance to be calculated in various areas of vanadium phase diagram. Figure 6, *a* shows calculated isobars *3* at GPa-scale pressures and thousand-degree temperatures. As can be seen, curves *3* in Figure 6, *a* in line with (3) have an *s*-shaped temperature dependence of resistivity, which proves the effect of vanadium resistivity saturation not only at atmospheric pressure, but also when the pressure increases up to tens of GPa.

Lets compare now the results of our model and literature shock-wave experiments. In Figure 6, *a*, dots *4* represent experimentally calculated resistivity of shock-compressed vanadium from TABLE I in [12]. It can be seen that dots *4* are appropriately placed among our model isobars *3*. This pattern is in that dots *4* are alternatively placed virtually on our model isobars *3* as the corresponding pressures in [12] increase from 17 to 50 GPa

Thus, general qualitative and quantitative agreement between the model results and our experimental results and experiment [12] in volume-temperature dependence of vanadium resistance supports the assumption that the effect of vanadium resistivity saturation is maintained at high pressures.

Let us now consider the use of the obtained results in relation to model calculations of the volume-temperature dependence of the electronic component of the vanadium thermal conductivity coefficient on the basis of the Wiedemann–Franz law $k_e = LT/\rho$ with a theoretical value of L for degenerate electronic gas $L = \text{const} = 2.45 \cdot 10^{-8}\,\mathrm{W\Omega/K^2}$ and lattice component of the Dugdal–Macdonald thermal conductivity k_l.

Calculation of k_e using the tabular parameters and equation of state was performed along the high-temperature atmospheric isobar of vanadium and is represented by curve *1* in Figure 6, *b*. The same figure shows experimental data *2* from [13]. It can be seen that curve *1* is considerably lower than experiment *2*. However, it turns out that this difference may be neutralized provided that the contribution of volume-temperature dependence o the lattice thermal conductivity k_l is taken into account similarly to [11].

Indeed, complete expression for the volume-temperature dependence of thermal conductivity for vanadium $k = k(V, T)$ is written as

$$k = k_e + k_l, \tag{5}$$

where, as above, $k_e = LT/\rho$ is the electronic component of thermal conductivity calculated according to the Wiedemann–Franz law with $L = \text{const} = 2.45 \cdot 10^{-8}\,\mathrm{W\Omega/K^2}$, and the second term is the Dugdal–Macdonald model expression of volume-temperature dependence of lattice thermal conductivity $k_l = k_l(V, T)$

$$k_l = k_{0l}\left(\frac{T_0}{T}\right)\left(\frac{V}{V_0}\right)\left(\frac{\Theta}{\Theta_0}\right)^3\left(\frac{\gamma_0}{\gamma}\right)^2. \tag{6}$$

Functions

$$\Theta = \Theta_0\left(\frac{\nu_0 - V}{\nu_0 - V_0}\right)^2\left(\frac{V_0}{V}\right)^{2/3}$$

and

$$\gamma = \frac{2}{3} + \frac{2V}{\nu_0 - V},$$

and $\gamma_0 = \gamma(V_0)$ in (6), similar to the data in [11], contain the known ν_0 and V_0. For vanadium, these parameters are listed in the table. k_{0l} is an adjustable parameter used to match the model calculations (5) with the experiment from [13]. In Figure 6, *b*, lower curve *3* represents the calculation of $k = k(V, T)$ according to (5) along the atmospheric isobar with the values of all parameters taken from the table. As we can see, the model calculation in the temperature range of 500–1300 K, taking into account the equation of state of vanadium, almost coincide with the experimental data *2* from [13].

It appears that matching up of the model calculations with the literature data in terms of the thermal conductivity coefficient at atmospheric pressure in Figure 6, *b* may be treated as verification of the proposed model of volume-temperature dependence of resistivity for vanadium.

Similarly to the resistance prediction, thermal conductivity isobars were predicted for vanadium in a high pressure range of 20–60 GPa and temperature range of 500–1300 K. This prediction is shown by upper curves *3* in Figure 6, *b*. It is seen that, for example, at $T = 700\,\mathrm{K}$ the pressure effect on the thermal conductivity coefficient of vanadium is$\approx 0.45\,\mathrm{W/(mK)}$ per 1 GPa.

Finally, note that no experimental data for the thermal conductivity coefficient of vanadium in the studied high pressure region was found in the available literature. Therefore, the calculated volume-temperature dependence of the thermal conductivity for vanadium in the high pressure region is predictive.

5. Conclusion

Electrical resistances of BCC polymorphous modification of vanadium were measured in a pressure range of20−60 GPa and temperature range of 580−730 K in stage-cyclic shock compression conditions.

Semi-empirical model of volume-temperature dependence of resistivity with vanadium temperature saturation at pressures up to tens of GPa and temperatures up to thousands of degrees was developed and verified. It is shown that the vanadium resistivity saturation effect taking place at atmospheric pressure is also maintained at GPa pressures.

The volume-temperature dependence of vanadium resistivity in the pressure range of 20−60 GPa and temperature range of 580−730 K was reconstructed.

Semi-empirical version of the patterns of volume-temperature dependence of thermal conductivity for vanadium was formulated at pressures up to tens of GPa and temperatures up to thousands of degrees.

Pressure-temperature dependence of the thermal conductivity coefficient of vanadium was predicted quantitatively in the pressure range of 0−60 GPa and temperature range of 500−1300 K.

Funding

The work was performed under state assignment № 124020600049-8.

Conflict of interest

The authors declare no conflict of interest.

References

[1] V.F. Gantmacher. Elektrony v neuporyadochennykh sredakh. Fizmatlit, M. (2013). 288 p. (in Russian).

[2] B. Sundqvist. J. Phys. Chem. Solids **165**, 110686 (2022).

[3] H. Inoue, S. Suehiro, K. Ohta, K. Hirose, Y. Ohishi. Earth Planet. Sci. Lett. **543**, 116357 (2020).

[4] P.D. Desai, H.M. James, C.Y. Ho. J. Phys. Chem. Ref. Data **13**, 1097 (1984).

[5] A.M. Molodets, A.A. Golyshev. Fizika Zemli, **4**, 39 (2024). (in Russian).

[6] A.M. Molodets, A.A. Golyshev, D.V. Shakhray. J. Phys.: Conf. Series **774**, 012008 (2016).

[7] J.M. Foster, A.J. Comley, G.S. Case, P. Avraam, S.D. Rothman, A. Higginbotham, E.K.R. Floyd, E.T. Gumbrell, J.J.D. Luis, D. McGonegle, N.T. Park, L.J. Peacock, C.P. Poulter, M.J. Suggit, J.S. Wark. J. Appl. Phys. **122**, 025117 (2017).

[8] D. Errandonea, S.G. MacLeod, L. Burakovsky, D. Santamaria-Perez, J.E. Proctor, H. Cynn, M. Mezouar. Phys. Rev. B **100**, 094111 (2019).

[9] C.T Seagle, E. Cottrell, Y. Fei, D.R. Huer, V.B. Prakapenka. Geophys. Res. Lett. **40**, 5377 (2013).

[10] A.M. Molodets, A.A. Golyshev. ZhTF **91**, *9*, 1403 (2021). (in Russian).

[11] A.M. Molodets, A.A. Golyshev, A.S. Savinykh, G.V. Garkushin. FTT **66**, *10*, 1763 (2024). (in Russian).

[12] Y. Wang, J. Li, J. Gao, Y. Zhang, W. Song, B. Gan, Y. Zhang. Phys. Rev. B **111**, 134101 (2025).

[13] L.K. Voronin, A.N. Merkulev, B.E. Neimark. Teplofizika vysikikh temperatur **8**, *4*, 780 (1979). (in Rissian).

Translated by EgoTranslating